Astron. Astrophys. 328, 107–120 (1997)

ASTRONOMY
AND
ASTROPHYSICS

Wolf-Rayet stars and OB assoctations as gamma-ray line sources

E. Parizot[1], **M. Cassé**[1,2], **and E. Vangioni-Flam**[2]

[1] Service d'astrophysique, CEA-Saclay, F-91191 Gif-sur-Yvette, France
[2] Institut d'Astrophysique de Paris, CNRS, 98bis bd Arago, F-75014 Paris, France

Received 18 April 1997 / Accepted 24 July 1997

Abstract. We calculate the gamma-ray line production induced by energetic particles (EPs) in molecular clouds where massive star formation is taking place, assuming that the EPs originate from the winds of these stars. On the basis of recent Wolf-Rayet (W-R) models of the Geneva group, we analyse in detail the average composition of the winds from OB associations. We consider two initial stellar metallicities (solar and twice solar), and study the metallicity dependence of the gamma-ray line ratios and profiles. In particular, we find that the gamma-ray lines are narrower at twice solar metallicity, which is of interest for the emission from the inner Galaxy. We pay particular attention to the gamma-ray emission detected by COMPTEL in Orion, and show that our mean-wind EP compositions satisfy all the available observational constraints. We predict a flux of 1-2 10^{-5} ph.cm^{-2}s^{-1} at $\sim$ 0.450 MeV from the Orion complex, due to the de-excitation of the spallation products ^{7}Li and ^{7}Be. Such a flux is below the current OSSE upper limit, but above INTEGRAL's expected sensitivity. We analyse the most relevant present and future observables, such as the broad band ratios (0.2-1 / 1-3 / 3-7 MeV), the ^{12}C and ^{16}O line width and the C*/O* line ratio, and discuss the differences between our results and those obtained with a WC composition based only on the extreme late phase wind, used up to now.

Key words: gamma rays: theory – nuclear reactions – interstellar medium: clouds: Orion – stars: Wolf-Rayet, mass loss – OB associations

1. Introduction

The gamma-ray emission in the 3-7 MeV range observed by COMPTEL from the Orion complex (Bloemen et al. 1994) and recently confirmed at a level of $\sim$ 1.3 10^{-4} ph.cm^{-2}.s^{-1} (Bloemen et al. 1997) has given rise to many analyses and discussions (e.g. Bykov & Bloemen 1994, Cassé et al. 1995, Ramaty et al. 1995). It is generally believed that this gamma-ray emission is due to in-flight de-excitation of fast ^{12}C and ^{16}O nuclei following their excitation to the 4.4 MeV and 6.1 MeV levels, respectively, by collision with the cloud material. The energetic particles involved seem to constitute a component on its own, distinct from the usual Galactic cosmic rays (GCRs), having notably a lower caracteristic energy ($\sim$ 10-30 MeV/n), a composition richer in carbon and oxygen, and an energy density higher by at least a factor of 10 (Ramaty 1996). We shall denote by EPs these energetic particles presumably associated with the intense mechanical activity (SNe and stellar winds, essentially) in regions of massive star formation, of which the Orion complex is the most vivid example.

Various energetic particle (EP) compositions have been studied in the context of the Orion gamma-ray emission (Cassé et al. 1995; Ramaty et al. 1995, 1996). Energetic considerations as well as the absence of any detected line between 1 and 3 MeV suggest that the EPs are helium poor and almost devoid of protons (Ramaty et al. 1995ab). On this basis, three compositions have been elected by Ramaty and co-workers, corresponding to three possible origins: carbon rich Wolf-Rayet (W-R) stars, supernovae with massive progenitors ($\sim 60\,M_{\odot}$) and interstellar grains (GR). SN and W-R compositions have also been used by Cassé et al. (1995) and Vangioni-Flam et al. (1996,1997) to evaluate the Li, Be and B (LiBeB) production in the interstellar medium (ISM) as a result of spallation reactions induced by EPs. The most attractive feature of such compositions enriched in freshly synthesized C and O is that they provide a natural understanding of the observed linear growth of the Be and B abundances in the early Galaxy, with respect to Fe, whereas GCR-produced Be and B grow quadratically with metallicity (Cassé et al. 1995).

In this article, we analyse in detail the expected composition of the EPs, considering that they result from the acceleration of the cumulated wind material blown by massive stars, and investigate the induced gamma-ray line emission. Although we have developed elsewhere time-dependent models adapted to the study of individual W-R stars and SNe (Parizot et al. 1997a,b,c), we assume here that nuclei injected by mass losing stars are continuously accelerated by large scale motions in regions experiencing a large energy release in the form of strong stellar winds and multiple supernova explosions (Bykov 1995, Bykov & Fleishman 1992). Therefore we use a steady-

state, thick target model, and study systematically the influence of both EP composition and target metallicity.

The main features of the present work are that: 1) we use integrated wind compositions instead of the surface composition of a WC star at the very end of its life (as done by Ramaty et al.), which represents only a negligible mass fraction of the wind, 2) we consider the mean composition of the combined ejecta of a whole OB association, 3) we extend our calculations to metallicities higher than solar in a consistent way, changing both the target composition (ambient material) and the EP composition. Indeed, the composition of a stellar wind depends on the initial metallicity of the star considered, while the target composition is basically the same as that of the material from which the star was formed, since the ambient chemical composition is nearly constant during the lifetime of the most massive stars. Accordingly, we use EP compositions deduced from massive star evolutionary models calculated at the same initial metallicity as that assumed for the target. In particular, the calculations at solar metallicity apply to Orion, while those at supersolar metallicity are assumed to describe the inner Galaxy.

2. Composition of the EPs

2.1. Mean-wind compositions

Leaving aside selective effects at the acceleration related to the different mass-to-charge ratios of the ions (Ellison et al. 1997, Meyer et al. 1997), we assume that the composition of the accelerated nuclei reflects the Wolf-Rayet stellar wind supplying the acceleration process. However, since we adopt the steady-state approximation, we must average the wind composition over the entire life of the star, weighting each instantaneous composition by the current mass loss rate. The total mass of the nuclear species i blown by the star during its life is given by:

$$M_i = \int_{\text{whole life}} \dot{M}(t)\, X_i(t) \mathrm{d}t \qquad (1)$$

where $\dot{M}(t)$ and $X_i(t)$ are respectively the stellar mass loss rate and the mass fraction of element i in the wind at time t.

We have estimated in this way the mean wind composition for stars with zero-age-main-sequence (ZAMS) masses $M_\star$ = 40, 60, 85 and 120 $\mathrm{M}_\odot$, using the massive star evolutionary models of the Geneva group (Schaller et al. 1992, Meynet et al. 1994), either with 'standard' mass loss rates (models C), mass-loss rates twice as large after the main-sequence phase (models D), or mass-loss rates twice as large during the main-sequence and the late WN phases (models E). Some of the resulting compositions, normalised to ^{16}O, are shown in Table 1.

In the special case of Orion, the study of the stellar content of the molecular complex has been carried out in great detail (e.g. Brown et al. 1994). Blaauw (1964) divided the Orion OB1 association into four subgroups: 1a, 1b, 1c and 1d, whose respective ages have been re-estimated recently to be (11.4 ± 1.9 Myr), (1.7 ± 1.1 Myr), (4.6 ± 2.0 Myr) and (< 1.0 Myr) respectively (Brown et al. 1994). The most recent intense activity is expected to be related mainly to subgroup 1c. Indeed, the most massive stars (with lifetimes $\leq$ 5 10^6 years) of subgroup 1a have exploded some 5-6 10^6 years ago, while the subgroups 1b and 1d are too young for even their most massive stars to have evolved up to the WC stage. Subgroup 1b actually contains the most massive stars known in Orion OB1, namely ζ Ori A (49 $\mathrm{M}_\odot$), δ Ori A (45 $\mathrm{M}_\odot$) and ϵ Ori A (42 $\mathrm{M}_\odot$), which are not observed as Wolf-Rayet stars. By contrast, subgroup 1c has just the age required for the stars of ZAMS mass $\sim$ 60 $\mathrm{M}_\odot$ (if any) to have exploded, but not the stars of $\sim$ 40 $\mathrm{M}_\odot$ (see Table 2). The most massive stars in OB1c are indeed ι Ori A (36 $\mathrm{M}_\odot$) and κ Ori (33 $\mathrm{M}_\odot$) (Lamers & Leitherer 1993; Vilkoviskij & Tambovtseva 1992). We conclude that the composition of the Orion EPs is likely to be of the 60 $\mathrm{M}_\odot$ mean-wind type.

Other compositions have been investigated in previous works. Ramaty et al. (1996) (hereafter RKL96) have discussed in detail the cases of solar system composition (SS), cosmic-ray source (CRS), supernova ejecta from stars of 35 $\mathrm{M}_\odot$ (SN35) and 60 $\mathrm{M}_\odot$ (SN60), dust grains (GR) and Wolf-Rayet (W-R) stars of spectral type WC. We also used these compositions comparison, and obtained identical results for both gamma-ray line and LiBeB production, except in the calculation of the (1-3 MeV)/(3-7 MeV) band ratio, to be discussed in Sect. 5.2.

It can be seen in Table 1 that the abundances of ^{1}H and ^{4}He are between one and two orders of magnitude lower in the 'WC' composition than in our mean-wind compositions (depending on the model used). This is because Ramaty et al. use the extreme late phase wind of a W-R star, whereas we use averaged abundances. However, the late WC composition should not reflect the mean EP composition, since the mass ejected from the star during the final episode is negligible with respect to the total mass of the wind. Indeed, the mass loss rate is highest at the onset of the W-R phase, when the wind is still rich in helium. Afterwards, the ^{4}He abundance in the wind continues to decrease, to the benefit of ^{16}O. As a consequence, the C/O ratio decreases by about a factor of 4 from the onset of the W-R phase to its very end, which also explains why our mean wind compositions have a higher C/O ratio than the 'late-WC' composition used by RKL96. This constitutes a second distinctive feature whose observational consequences, together with those of the higher ^{1}H and ^{4}He abundances, are discussed below.

2.2. Mean-OB compositions

In the general situation where nuclei are accelerated from the hot plasma filling a bubble (or superbubble) created by joint stellar winds and multiple SNe, as possibly in Orion (Cowie et al. 1979, Burrows et al. 1993, Bykov & Bloemen 1994), the mean wind compositions of individual stars are probably not appropriate. Rather we have to consider a global mean composition, arising from an evolved OB association. To obtain such a 'mean-OB' composition, we must weight the mean-wind composition of each star in a given range of ZAMS mass according to its total ejected mass and to its probability of occurrence among the association, which is given by the initial mass function (IMF). Indeed, the most massive stars supply the bubble with more

Table 1. Mean wind and mean OB compositions assumed for the EPs

isotope	$40M_\odot$/C	$60M_\odot$/C	$60M_\odot$/D	$60M_\odot$/E	$85M_\odot$/C	late-WC[1]	OB/0.02	OB/0.04
^{1}H	8.03e+01	5.76e+01	1.48e+02	1.61e+02	2.85e+01	1.00	5.32e+01	1.21e+02
^{4}He	2.52e+01	1.91e+01	7.98e+01	6.42e+01	9.29e+00	9.20e-01	1.71e+01	5.63e+01
^{12}C	1.59	2.57e+00	5.66e+00	4.78e+00	1.63e+00	6.90e-01	1.88e+00	3.79e+00
^{13}C	1.15e-03	6.88e-04	2.34e-03	2.09e-03	2.73e-04	0.00	6.69e-04	4.29e-03
^{14}N	1.08e-01	4.60e-02	2.00e-01	2.11e-01	2.92e-02	2.40e-03	5.90e-02	3.56e-01
^{16}O	1.00	1.00	1.00	1.00	1.00	1.00	1.00	1.00
^{20}Ne	1.56e-02	1.30e-02	3.97e-02	3.53e-02	7.27e-03	2.30e-03	1.15e-02	5.95e-02
^{22}Ne	4.52e-02	7.66e-02	2.21e-01	1.83e-01	4.83e-02	2.00e-02	5.53e-02	2.78e-01
^{24}Mg	4.71e-03	3.94e-03	1.20e-02	1.07e-02	2.21e-03	6.30e-04	3.50e-03	1.81e-02
^{25}Mg	5.94e-04	4.97e-04	1.52e-03	1.35e-03	2.79e-04	0.00	4.41e-04	2.28e-03
^{26}Mg	5.49e-04	1.67e-03	1.49e-03	1.49e-03	4.00e-03	5.32e-03	4.87e-04	2.52e-03
^{27}Al	4.71e-04	3.95e-04	1.20e-03	1.07e-03	2.22e-04	6.70e-05	3.50e-04	1.81e-03
^{28}Si	5.12e-03	4.29e-03	1.31e-02	1.17e-02	2.41e-03	6.90e-04	3.80e-03	1.97e-02
^{32}S	2.71e-03	2.27e-03	6.93e-03	6.19e-03	1.28e-03	3.30e-04	2.02e-03	1.04e-02
^{40}Ca	3.29e-04	2.75e-04	8.40e-04	7.49e-04	1.55e-04	5.00e-05	2.44e-04	1.26e-03
^{56}Fe	4.45e-03	3.72e-03	1.14e-02	1.01e-02	2.09e-03	9.10e-04	3.30e-03	1.71e-02

[1] From Ramaty, Koszlovsky & Lingenfelter (1996)

enriched material than the lighter ones, but on the other hand they are less numerous.

The mean OB compositions are thus obtained from the total ejected mass of isotope i:

$$M_i^{\rm tot} = \int_{M_{\rm inf}}^{M_{\rm sup}} N(M_\star)\ M_i(M_\star) {\rm d}M_\star \qquad (2)$$

where $N(M_\star) = K M_\star^{-(x+1)}$ is the IMF, and $M_i(M_\star) = X_i(M_\star)\ \Delta M_w(M_\star)$. A few examples of total mass loss $\Delta M_w(M_\star)$, taken from the Geneva group calculations, are shown in Table 2.

The resulting compositions are quite independent of $M_{\rm sup}$, the mass of the heaviest stars which contribute, because these stars are very rare, even in the case of a hard IMF with index $x = 1$. Here we set $M_{\rm sup} = 120\,{\rm M}_\odot$. Concerning $M_{\rm inf}$, we argue that most of the energy released within superbubbles comes from stars with mass greater than $\sim 40\,{\rm M}_\odot$. Since less massive stars have longer lifetimes, the contribution of their winds is expected to come too late to participate to the acceleration process. We thus assume here that $M_{\rm inf} = 40\,{\rm M}_\odot$, and argue that, accordingly, the OB associations should not be active as gamma-ray line sources during more than ~ 5 Myr, the lifetime of $40\,{\rm M}_\odot$ stars (see Table 2).

However, we also investigated as an 'extreme case' various EP compositions obtained with $M_{\rm inf} = 20\,{\rm M}_\odot$. In a general way, these compositions are poorer in C and O, with respect to H and He, and have a smaller C/O abundance ratio than the 'standard' compositions obtained with $M_{\rm inf} = 40\,{\rm M}_\odot$. Both cases are compared in Sect. 8. However, our main conclusions are found to be insensitive to such a change in $M_{\rm inf}$.

Table 2. Total mass loss ΔM and lifetime T of massive stars for different metallicities Z and initial masses (ZAMS). Models C, D and E are defined in the text.

model/Z	C/0.02	D/0.02	E/0.02	C/0.04
ZAMS	ΔM ($M_\odot$) /T (Myr)			
$20\,{\rm M}_\odot$	3.5/9.0	6.0/9.0	6.5/9.0	4.5/7.7
$25\,{\rm M}_\odot$	4.4/7.1	14/7.1	15/7.1	13/6.1
$40\,{\rm M}_\odot$	32/4.8	36/4.9	35/5.0	34/4.3
$60\,{\rm M}_\odot$	52/3.9	57/4.2	54/4.0	54/3.5
$85\,{\rm M}_\odot$	76/3.2	82/3.4	80/3.6	79/3.1
$120\,{\rm M}_\odot$	112/3.0	118/3.5	116/3.9	114/2.9

In Table 1 we show mean-OB compositions calculated for solar and twice solar metallicities, recalling that the first composition applies to Orion and the second one to OB associations in the inner Galaxy. The assumed IMF index is $x = 1.7$, which is the value estimated for the Orion OB1 association (Brown et al. 1994). The stellar evolutionary models that we use are again those of the Geneva group, and the compositions shown in Table 1 correspond to standard mass loss rates (models C). Other models and IMF indices have been investigated, but we do not show them here.

It is worth noting that: i) as Z increases, the WC-O phase arises earlier and earlier in the stellar evolution, when ^{4}He has only burned partially in the core. In our example of a $60\,{\rm M}_\odot$ star, only 50% of the core ^{4}He has burned at the onset of the WC phase (i.e. when the mass loss rate is highest) for $Z = 0.02$, and only 30% for $Z = 0.04$. As a consequence, the metals are relatively less abundant in the winds of twice solar metallicity

Table 3. Masses (in $M_\odot$) of H, He, C and O lost by a $60\,M_\odot$.

	H	He	C	O
Integrated wind	16.9	22.4	9.1	4.7
SN explosion	0.	0.21	0.53	1.38

stars than in the winds of solar metallicity stars. ii) a higher C/O ratio occurs for $Z = 0.04$; not as much carbon is burned into oxygen, since some of it is expelled - and thus saved - in the wind. Some implications of these pecularities are analysed below.

2.3. Remark on the W-R models

We have assumed that the EP composition reflects essentially that of the winds of massive stars, neglecting in particular the supernovae ejecta contribution. This is justified in the case of Orion, since the total mass lost by a massive star during its life is much larger than the mass ejected in its final explosion (see Table 2). We also compare in Table 3 the masses of the most relevant nuclei expelled in the wind and in the explosion by a $60\,M_\odot$ star, using the wind model C and the explosion model WRA of Woosley et al. (1993). Note that the SN ejecta are very rich in ^{16}O, and might enhance somewhat the oxygen abundance in the EPs, and in turn lower slightly the $^{12}C^*/^{16}O^*$ emission line ratio.

3. EPs energy spectrum

Apart from the EP composition, the energy spectrum of the EPs must be specified in order to calculate the gamma-ray line shapes and ratios from EP interactions in the cloud material. In the case of Orion, however, no decisive information can be drawn from the gamma-ray line shapes. This is due to the poor energy resolution of the instruments and to the ambiguity on the EP composition itself. On the other hand, the gamma-ray emission at higher energy ($\gtrsim$ 100 MeV), due to π^0 decay principally, has been measured first by COS-B (Bloemen et al. 1984), and most recently by EGRET (Digel et al. 1995) and was found compatible with the GCR flux observed at Earth. This strongly suggests that the energy spectrum of the extra EP component breaks at an energy lower than the π^0 production threshold of a few hundreds MeV/n.

It is quite remarkable that independently of these phenomenological considerations, and actually before the observations by COMPTEL of the gamma-ray line emission in Orion, Bykov & Toptygin (1990) and Bykov & Fleishman (1992) presented a model of 'non-thermal particle generation in superbubbles' leading to hard spectra of energetic nuclei up to tens or hundreds of MeV. Their calculated spectra (see also Bykov 1995) are rather similar to that adopted by Ramaty and co-workers on the basis of shock acceleration calculations (e.g. Ellison & Ramaty 1985) with a finite acceleration time or a finite shock size:

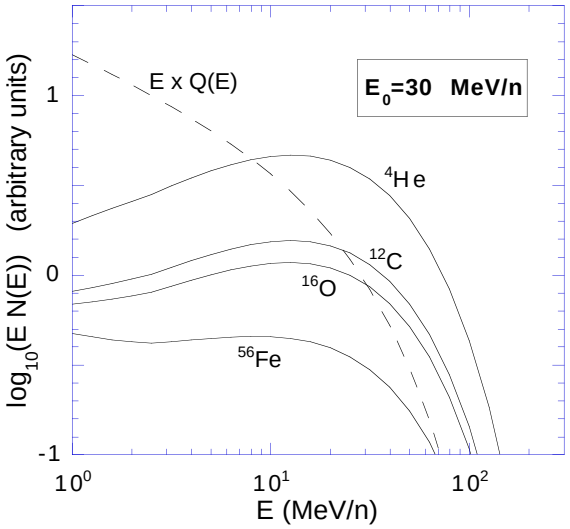

Fig. 1. Energy content of the propagated EP spectrum for different nuclei and for E_0 = 30 MeV/n. We also show the same quantity for the injected spectrum (dashed line), with arbitrary relative scale. All the nuclear species have the same abundance at injection.

$$Q_i(E) = K_i \left(\frac{E}{E_0}\right)^{-1.5} exp\left(-\frac{E}{E_0}\right) \quad (3)$$

As emphasized e.g. in RKL96, this analytical form allows one to explore a variety of phenomenologically possible spectra by varying one single parameter, namely the 'break energy' E_0. Therefore we adopt this formalism, varying E_0 from 2 to 100 MeV. The normalisation coefficients K_i, are proportional to the abundances by number of each isotope i, according to the compositions discussed in Sect. 2. Finally, we normalise the EP spectra so as to reproduce the detected flux from Orion in the range 3-7 MeV, i.e. $\sim 1.3\,10^{-4}$ ph.cm^{-2}s^{-1} (Bloemen et al. 1997).

Knowing the injection function $Q_i(E)$, one can derive the 'propagated' energy spectrum $N_i(E)$ of EP species i from the usual transport equation:

$$\frac{\partial}{\partial t}N_i(E,t) + \frac{\partial}{\partial E}(\dot{E}_{\rm ion}(E)N_i(E,t)) = Q_i(E,t) - \frac{N_i(E,t)}{\tau_i} \quad (4)$$

where τ_i is the total lifetime of nuclei i against catastrophic losses (escape, nuclear destruction and/or decay). In the steady-state approximation, we have:

$$N_i(E) = \frac{1}{\left|\dot{E}(E)\right|}\int_E^{+\infty} Q_i(E_0)\,\exp\left(-\frac{1}{\tau_i}\int_{E_0}^{E}\frac{{\rm d}E'}{\dot{E}_{\rm ion}(E')}\right){\rm d}E_0 \quad (5)$$

In Fig. 1, we show the energy distribution of different nuclei, $E\,N_i(E)$, representing the amount of energy between E and $E+$

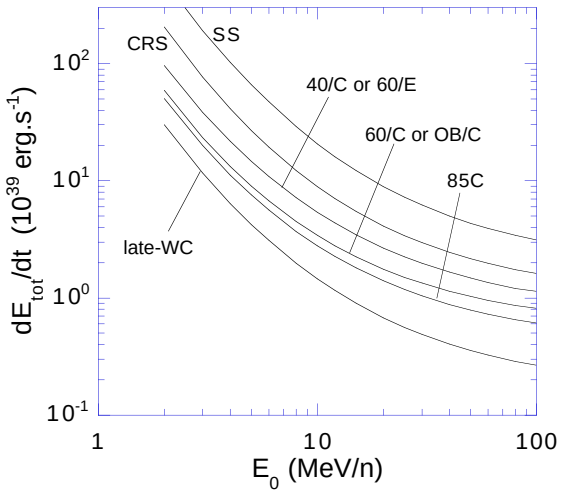

Fig. 2. Ionisation energy losses (in units of 10^{39} erg.s^{-1} as a function of the break energy E_0, for different EP compositions. For example, 60/E refers to the mean-wind of a 60 $M_\odot$ star with model E. The target composition is solar.

dE. For clarity, all the nuclear species have been given the same abundance at injection, so that the differences between nuclei are only due to their different energy losses, as a consequence of their different Z^2/A ratio. We also plot the same quantity for the injection spectrum, i.e.$E\,Q_i(E)$.

Although the injected energy is a monotonically decreasing function of energy, it appears that the energy of the propagated EPs is concentrated around the break energy of the injection spectrum. This indicates that the gamma-ray emission is mainly governed by the relative behaviour of the different cross sections of interest at energies around the break energy.

Because of their interactions in the surrounding medium, the EPs suffer ionisation energy losses, at a rate:

$$\left.\frac{dE_{\rm tot}}{dt}\right|_{\rm ion} = \sum_i \int N_i(E)\ \rho\, v(E) \left.\frac{dE}{dx}\right|_{\rm ion}(E)\, dE \qquad (6)$$

The discrete sum is over all EP species, ρ is the mean density of the interaction region, $v(E)$ is the velocity of the particles, and $(dE/dx)_{\rm ion}$ is the ionisation energy loss per g.cm^{-2}.

The energy loss rate of the EPs and the gamma-ray production rates are both proportional to the ISM density (see Eq. 7). Therefore, the normalisation to the Orion fluxes allows us to obtain absolute (i.e. density independent) energy loss rates, which are shown in Fig. 2 as a function of the break energy E_0 of the injection spectrum. For the sake of clarity, we only plot the results for a few representative mean-wind compositions, including the solar system (SS) and late-WC compositions, for comparison. The gamma-ray production efficiency is higher for larger values of E_0, since: i) more particles are above the excitation thresholds and ii) the ionisation energy losses are lower at higher energies. However, this effect is compensated by the decrease of the excitation cross sections above $\sim$ 30 MeV/n, which explains the flatening of the curves in Fig. 2.

In a general way, all the compositions that we consider provide gamma-ray emission efficiencies intermediate between the solar composition (the worse) and the late-WC composition (the best). This results from the higher proton and helium abundances in our mean-wind and mean-OB compositions as compared to the late-WC case, as discussed in Sect. 2. Indeed, since we normalise the EP energy spectrum to the gamma-ray flux emitted in the 3-7 MeV band, i.e. in first approximation to the ^{12}C and ^{16}O line fluxes (see Sect. 6), the highest efficiency is obtained for compositions having the highest C and O abundances.

It should be realised from Fig.2 that the gamma-ray fluxes detected from Orion actually imply a very high energy consumption within the cloud complex, namely $\sim 10^{39}$ erg.s^{-1} in the best case. This represents an energy of $\sim 3\,10^{51}$ erg over a period of 10^5 years. However, if the gamma-ray emission in Orion is to be attributed to the excitation of energetic C and O nuclei, one has to admit that nature actually manages to supply such a mechanism. Taking this as a fact, we shall focus on the implications of the detected Orion flux. The energetics will be discussed in a separate paper. Nevertheless, the energetic considerations favour values of E_0 greater than about 20 MeV/n. Moreover, they tend to exclude hydrogen and helium rich EP compositions, such as SS and probably also CRS compositions, as shown by Ramaty et al.

4. Gamma-ray line production

A given gamma-ray line can be obtained through several nuclear reactions, including direct excitation from protons and α particles, and production in an excited state by a spallation reaction. For each channel ($i + j \rightarrow \gamma$) with cross-section $\sigma_{ij;\gamma}$, we have:

$$\frac{dN_\gamma}{dt} = \int N_i(\,E)\, v(E)\, \rho_j\ \ \sigma_{ij;\gamma}(E)\, dE \qquad (7)$$

We use a wide sample of nuclear reactions based on the compilation by Ramaty et al. (1979) (hereafter RKL79), with more than 70 gamma-ray lines and almost 200 cross-sections (updated when possible; Tatischeff et al. 1996). However, only a few of these lines have significant contributions to the total emitted flux.

In the context of gamma-ray line spectroscopy, one has to distinguish between broad line and narrow line production mechanisms. The energy dispersion of the emitted gamma-rays reflects the velocity distribution of the excited nuclei with respect to the observer, that is, to a good approximation, with respect to the ISM. In the case of the interaction of light EPs (protons or α particles) with heavy ISM nuclei, the heavy excited nuclei, because of their large inertia, acquire a recoil velocity much lower than that of the projectile. The resulting de-excitation lines are then rather narrow in this case (width ranging from a few tens of keV to around 100 keV). We shall refer to this 'light-onto-heavy' process as the 'direct process'. Conversely, 'heavy-onto-light' interactions lead to heavy excited nuclei with velocities close to those of the incident EPs and produce in turn

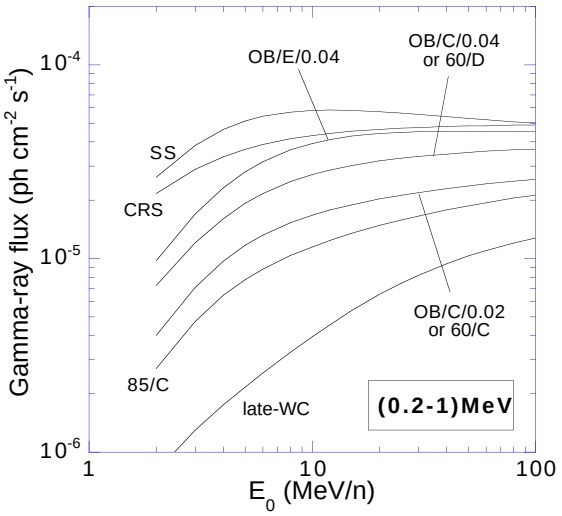

Fig. 3. Total gamma-ray flux in the 0.2-1 MeV band as a function of the injection break energy E_0 for different EP compositions. The fluxes are normalised to the Orion flux in the 3-7 MeV band. The target metallicity is $Z = 0.02$, unless explicitly specified.

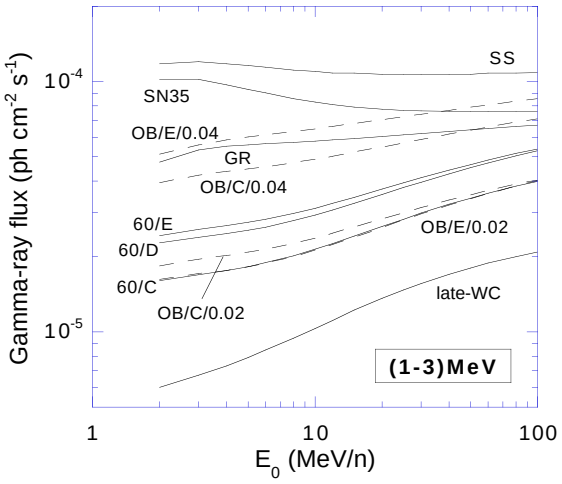

Fig. 4. Same as Fig. 3 for the 1-3 MeV band emission.

broad de-excitation lines (from a few hundreds of keV to an MeV). This will be refered to as the 'inverse process'.

5. Broad band integrated gamma-ray fluxes

The high resolution gamma-ray spectrometer SPI to be launched onboard INTEGRAL in the early 2000s should teach us much about the detailed nuclear processes responsible for the gamma-ray emission in Orion, and hopefully in other regions (Winkler 1997, Mandrou et al. 1997, Gehrels et al. 1997). However the broad band analysis available from the COMPTEL data can already provide some interesting information, and is also relevant to the INTEGRAL's imager IBIS (Ubertini et al. 1997).

5.1. The 0.2-1 *MeV band*

As we shall see in Sect. 7, apart from the ^{10}B spallation line at 0.717 MeV which dominates only for high values of E_0, the main contribution to the 0.2-1 MeV band emission is the ^{7}Li-^{7}Be feature around 0.450 MeV. Since it is mainly produced through α-α interactions, the emissivity is greater for EP compositions richer in α particles. As a consequence, the highest emission in this band is obtained for the SS composition, and the lowest for the late-WC one. In Fig. 3 we show the fluxes calculated for some intermediate EP compositions, namely our mean-wind and mean-OB compositions, at both solar ($Z = 0.02$) and twice solar ($Z = 0.04$) metallicity.

It can be seen that the (0.2-1 MeV)/(3-7 MeV) band ratio is enhanced by a factor of 1.5-2 at twice the solar metallicity. As a consequence, we predict a slight difference between the gamma-ray emission from Orion (solar metallicity) and that of the central radian of the Galaxy, dominated by the '4 kpc ring' where the metallicity is enhanced.

5.2. The 1-3 *MeV band*

Most of the nuclear gamma-ray lines, except those from ^{12}C and ^{16}O, are between 1 and 3 MeV. The (1-3 MeV)/(3-7 MeV) band ratio therefore depends mainly on the (C+O)/He abundance ratio in the EPs. Some typical results are shown in Fig. 4. Again, we see that the 1-3 MeV band emission is higher, or if one prefers, the 3-7 MeV band emission is lower by a factor of 1.5-3 for $Z = 2\,Z_\odot$. This is due to the fact that the ^{12}C and ^{16}O nuclei (producing the 3-7 MeV flux) have lower abundances in the winds of massive stars with higher initial metallicity, as explained in Sect. 2.2. This effect could also be of interest for future observations of diffuse gamma-ray line emission as a function of galactocentric longitude. Note in passing that the stellar evolutionary models using an enhanced mass loss rate during the MS phase lead to compositions richer in ^{1}H and ^{4}He (or poorer in ^{12}C and ^{16}O), and in turn to a slightly higher gamma-ray emission between 1 and 3 MeV.

The same conclusions can be drawn from Fig. 5, where we present essentially the same results in a slightly different way, in order to compare our calculations with the observations made by COMPTEL in Orion, as well as with previous calculations by Ramaty and co-workers (Ramaty 1996, RKL96). Indeed, the COMPTEL data set a 2σ upper limit of 0.13 on the band ratio R defined as:

$$R = 2\,\frac{\int_{1\,\mathrm{MeV}}^{3\,\mathrm{MeV}} E_\gamma^2 Q(E_\gamma)\mathrm{d}E_\gamma}{\int_{3\,\mathrm{MeV}}^{7\,\mathrm{MeV}} E_\gamma^2 Q(E_\gamma)\mathrm{d}E_\gamma} \qquad (8)$$

The results that we obtain depend on the way we deal with the so-called 'unresolved gamma-ray lines', discussed in RKL79. Nuclear interactions between energetic particles and complex nuclei (with $A \geq 20$) produce numerous gamma-ray lines resulting from transitions between many high-lying nuclear levels populated by both direct excitations and spallation reactions. The cross sections for the production of these lines have not been measured individually (hence the term 'unresolved'), but Zobel et al. (1968) measured the total production

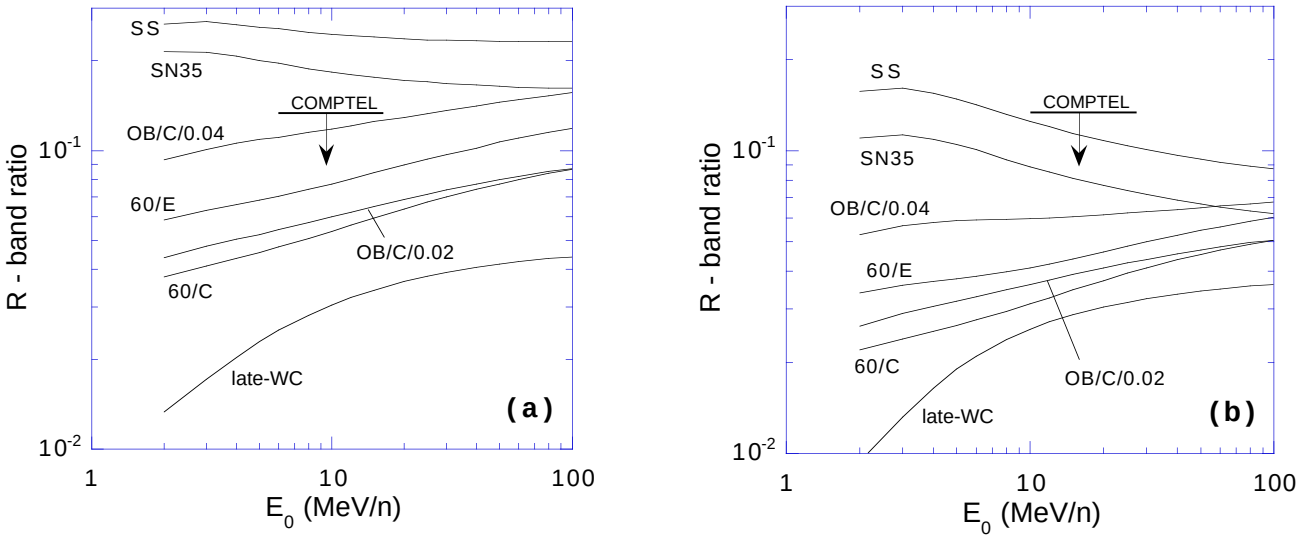

Fig. 5a and b. Evolution with the injection break energy E_0 of the (1-3 MeV)/(3-7 MeV) band ratio R defined in the text, for various EP compositions. In **a**, the unresolved gamma-ray lines are included, in **b**, they are not.

cross sections of gamma-rays of energies greater than 0.7 MeV. Now the value of the (1-3 MeV)/(3-7 MeV) band ratio depends on the distribution in energy of these unresolved gamma-rays. Estimations of this distribution for different nuclei are given in RKL79 (based on experimental data), showing a peak between 1 and 2 MeV. This peak is sharper for heavier nuclei. This is intuitively in agreement with the idea that high-lying levels are rather close to one another.

The results obtained with this prescription for the unresolved gamma-ray lines are shown in Fig. 5a. They are in very good agreement with the calculations of Ramaty and co-workers for any of our common compositions. The main result here is that all our mean-wind and mean-OB compositions lead to R band ratios compatible with available COMPTEL observations. This is important in itself since the R ratio proves to be very constraining in the case of Orion, excluding the most 'natural' EP compositions, such as SS or CRS (e.g. RKL96). In the same time, it justifies the investigation of the 'superbubble model' for the Orion gamma-ray line emission, discussed in Parizot (1997).

In order to stress the importance of the unresolved gamma-ray lines, we also calculated the R ratio taking into account only the resolved lines. The results are presented in Fig. 5b. They show that, in this case, no EP composition can be excluded anymore on the basis of the sole R ratio. This points out the major role of these (up to now) unresolved gamma-rays, and the astrophysical interest that would represent the precise measurement of the corresponding cross sections - at least to confirm the current estimates on the gamma-ray energy distribution. However, as argued by Ramaty (private communication), the same estimates have been used to model the solar flare emission, and the data were fit quite well (see Ramaty et al. 1997). This suggests that the estimates are actually good.

6. ^{12}C and ^{16}O lines and line ratio

Since ^{12}C and ^{16}O are the most abundant nuclei in the winds of massive stars after protons and α particles, the two most intense gamma-ray lines predicted are the ^{12}C line at 4.438 MeV and the ^{16}O line at 6.129 MeV, in agreement with the COMPTEL observations in Orion. These two lines also constitute the main contribution to the total gamma-ray flux emitted in the range 3-7 MeV, to which we have normalised all our calculated fluxes. We have used the updated cross sections of Tatischeff et al. (1996).

6.1. The ^{12}C line at 4.438 MeV

The first excited state of ^{12}C can be populated by direct excitation from EP-ISM interactions, or by the breaking of heavier nuclei in spallation reactions, mainly of ^{16}O and ^{14}N. For all the compositions considered here, however, the main contribution to the 4.438 MeV line is the in-flight excitation of energetic ^{12}C nuclei on ISM protons, leading to essentially broad line emission. Figs. 6 and 7 show the detailed contribution of all the production mechanisms representing more than 1 % of the total gamma-ray line flux, in two extreme cases. The first corresponds to the late-WC composition, which is so poor in protons and alpha particles that more than 99 % of the 4.438 MeV line flux is due to inverse reactions involving carbon and oxygen; and the second corresponds to the mean-wind composition of an OB association with twice solar initial metallicity and enhanced mass loss rates (Geneva group's model E). In this case direct reactions contribute to about 20 % of the total ^{12}C* production, and EP's ^{14}N nuclei excitation provides the second most important contribution to the gamma-ray line flux, for any break energy $E_0 \geq 25$ MeV/n.

In order to distinguish the broad and narrow components of the 4.438 MeV line (leaving aside the possible line splitting; Bykov et al. 1996, Ramaty et al. 1997), we show in Fig. 8 the

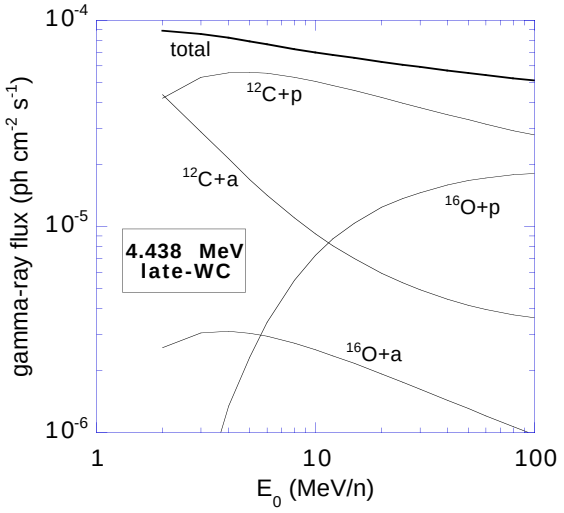

Fig. 6. Detailed production of the ^{12}C 4.438 MeV line as a function of the injection break energy E_0 for a late-WC composition with solar initial metallicity. The labels indicate the reactions considered, the first quoted species being the projectile.

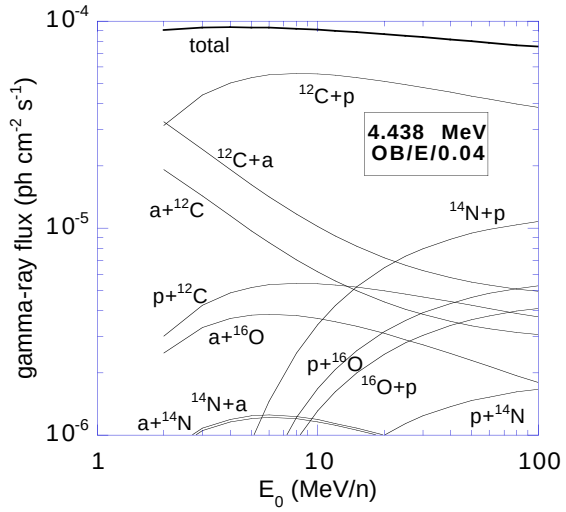

Fig. 7. Same as Fig. 6 for a mean-OB composition with models E and twice solar metallicity.

ratio of inverse to direct contributions for various EP compositions, excluding GR and late-WC compositions for which this ratio is greater than 100, as will as solar composition for which it is of order 0.3. The wide range of variation of this ratio demonstrates that any instrument capable of measuring the ^{12}C line profile, such as INTEGRAL's SPI, would be able to set strong constraints on the actual EP composition.

6.2. The ^{16}O line at 6.129 MeV

Fig. 9 and 10 show the detailed production of the 6.129 MeV line resulting from the de-excitation of ^{16}O nuclei produced in their first excited level by direct excitation and ^{20}Ne spallation for two EP compositions corresponding to the same model (mean-OB composition with models C and IMF index $x = 1.7$), but with either solar or twice solar initial metallicity. The differences are quite striking.

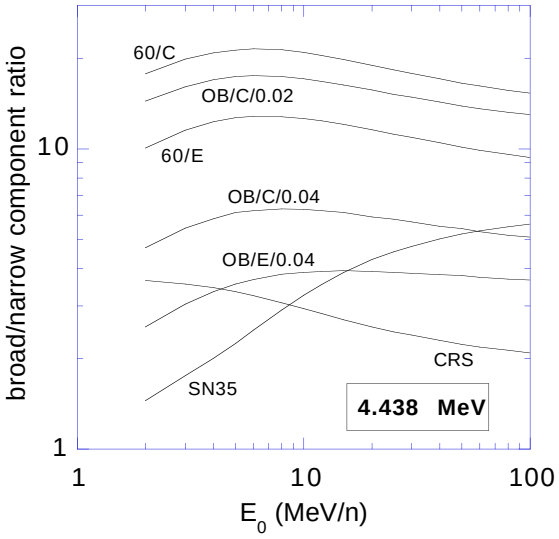

Fig. 8. Inverse-to-direct component ratio for the ^{12}C line at 4.438 MeV, for various EP compositions. The labels indicate the model and the metallicity used. The latter is solar unless explicitely specified.

In the case of solar initial metallicity, the EPs are much richer in ^{16}O than the ambient ISM (O/H= $1.9\,10^{-2}$ versus $8.5\,10^{-4}$). As a result, the encounters of energetic ^{16}O nuclei with ISM protons are much more frequent than that of energetic protons with ISM ^{16}O nuclei. This is not anymore the case at twice solar metallicity, because the EPs are richer in protons (O/H= $8.3\,10^{-3}$ versus $1.7\,10^{-3}$). As a consequence, direct and inverse excitations involving protons contribute to the gamma-ray line flux at about the same level (Fig. 10). This effect is even more pronounced for the α-^{16}O reactions, because of the strong enhancement of the mean-wind helium abundance when passing from solar to twice solar metallicity. The direct-to-inverse ratio then reverses, resulting in a dominating narrow line emission. This prediction could be tested by the variation of the ^{16}O line profile as a function of the Galactic longitude, since most of the metal-rich W-R stars should be concentrated in the 4 kpc ring.

Fig. 11 shows the global inverse-to-direct ratio, or equivalently the broad-to-narrow line component ratio for various EP compositions. As in the case of the ^{12}C line at 4.438 MeV, it can be seen that this ratio is very sensitive to the source composition.

At any rate, we predict a 6.129 MeV line significantly narrower than the 4.438 MeV line for any of our mean wind compositions (from either individual stars or OB associations). In particular, the direct reactions are always found to contribute to at least 20 % of the total line emission, and actually dominate in the case of a twice solar metallicity (inner Galaxy) or for models with enhanced mass loss rates during the main-sequence phase. This represents a distinctive feature of our models with

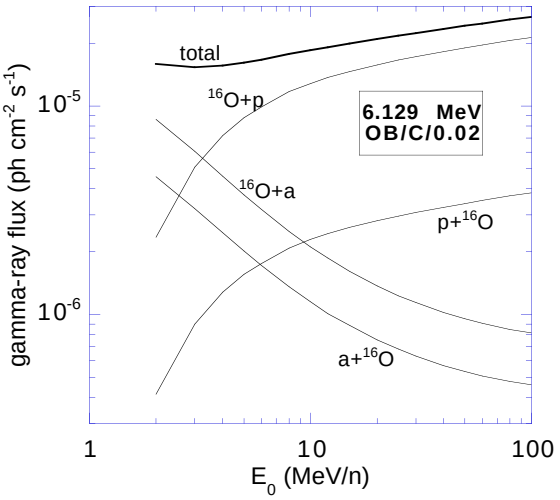

Fig. 9. Detailed production of the ^{16}O 6.129 MeV line as a function of the injection break energy E_0 for a mean-OB composition at solar metallicity.

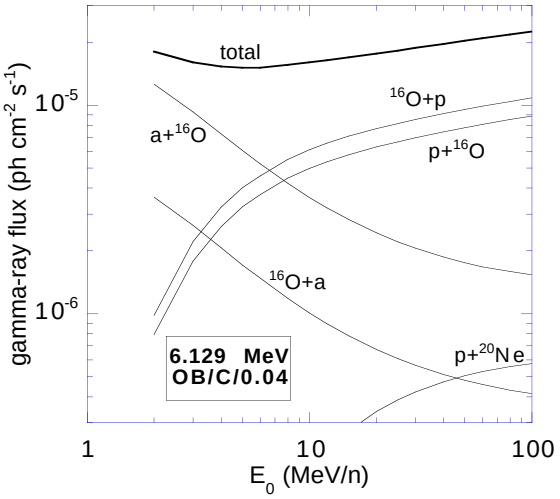

Fig. 10. Same as Fig. 9 at twice solar metallicity.

respect to, e.g., the late-WC model which presents a very high ^{16}O abundance.

6.3. The $^{12}C^*/^{16}O^*$ line ratio

Apart from the line profiles discussed above, the $^{12}C^*/^{16}O^*$ gamma-ray line ratio is one of the most relevant observable for gamma-ray spectroscopy. It should indeed be accessible quite easily to the INTEGRAL's spectrometer SPI in Orion, and also presumably in the diffuse Galactic emission. The data collected by COMPTEL provide a first constraint on this line ratio in Orion (Bloemen et al. 1997). Our rough guess estimate is $2 \leq {}^{12}C^*/{}^{16}O^* \leq 4$.

As can be seen in Fig. 12 and Fig. 13, the $^{12}C^*/^{16}O^*$ ratio is quite sensitive to the chemical composition of the EPs. If our rough estimate is correct, one can already exclude many

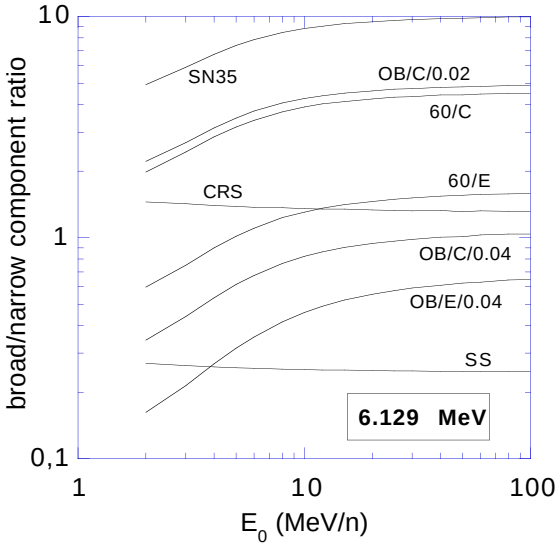

Fig. 11. Inverse to direct component ratio for the ^{16}O line at 6.129 MeV, for various EP compositions. The labels indicate the models and the metallicity used (solar metallicity unless explicitely specified.

compositions, among them the solar system (SS), grain (GR), 35 $M_\odot$ supernova ejecta (SN35), as well as late-WC compositions, whatever the value of the break energy E_0 may be. On the contrary, our mean-OB compositions seem to provide a more adequate line ratio. In the case of a 60 $M_\odot$ star with enhanced mass loss rate (model E), a break energy $E_0 \gtrsim 40$ MeV/n is required.

Although our estimate is admitedly uncertain, we point out that whatever the value of the $^{12}C^*/^{16}O^*$ line ratio will prove to be, its measurement will allow us to distinguish between mean-WC and late-WC compositions, and will provide a strong argument to exclude (or favour) compositions such as SS, GR or SN35.

Finally, we note that in a general way, the $^{12}C^*/^{16}O^*$ line ratio decreases for increasing values of the injection break energy E_0. This is due to the high excitation threshold of ^{16}O. However, this does not apply to the SN35 composition. In this case, indeed, the ^{16}O abundance is so high with respect to ^{12}C (~ 15 times greater) that the main contribution to the 4.438 MeV line is of spallative origin (except for the lowest values of E_0). Both ^{12}C and ^{16}O lines are thus due to the same collisions, namely ^{16}O+p, so that the previous argument doesn't hold.

7. The main other gamma-ray lines

Other gamma-ray lines produced by EP interactions in the ISM may be observed in the future thanks to more sensitive instruments such as INTEGRAL, or with longer COMPTEL exposures. In Fig. 14, we show the gamma-ray fluxes calculated for the most intense lines as a function of the break energy E_0, for different EP compositions relevant to the Orion complex as well as to the inner Galaxy. The fluxes are normalised to the Orion flux in the band 3-7 MeV. Only the lines with fluxes

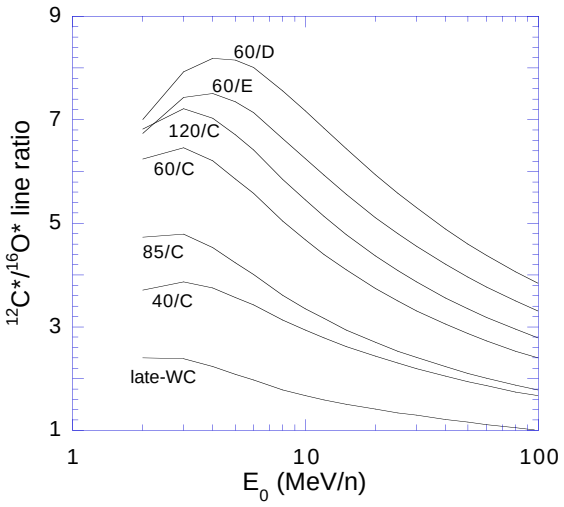

Fig. 12. $^{12}C^*/^{16}O^*$ gamma-ray line ratio as a function of the injection break energy E_0, for different EP compositions.

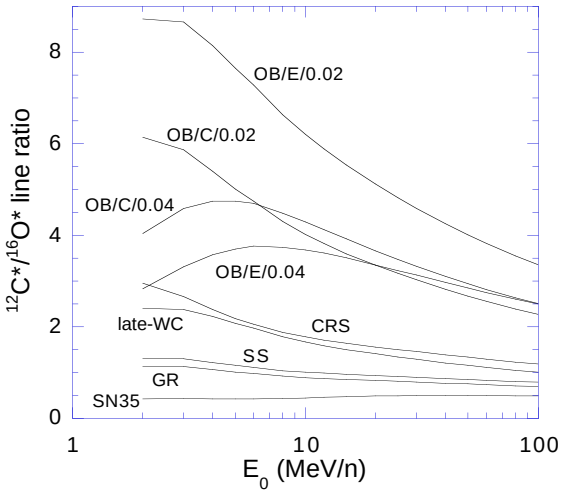

Fig. 13. Same as Fig. 12 with mean-wind compositions from individual stars.

greater than $2\,10^{-6}$ ph.cm^{-2}.s^{-1} are shown, recalling that INTEGRAL's sensitivity is expected around $5\,10^{-6}$ ph.cm^{-2}.s^{-1} for narrow lines and $5\,10^{-5}$ ph.cm^{-2}.s^{-1} for broad lines (Mandrou et al. 1997). Note for example that the lines from ^{24}Mg (1.369 MeV) and ^{28}Si (1.779 MeV) which are observed in solar flares (e.g. Murphy et al. 1991) are always weaker than $2\,10^{-6}$ ph.cm^{-2}.s^{-1} in the considered scenarii.

7.1. The ^{7}Li-^{7}Be feature at $\sim$ 0.450 MeV

The $\alpha+\alpha$ fusion reactions lead to significant production of ^{7}Li, either directly or through the decay of the unstable mirror nuclei ^{7}Be. In any case, these reactions are accompanied by gamma-ray emission. Some of the ^{7}Li nuclei are indeed produced in an excited state at 0.478 MeV, while 90% of the ^{7}Be nuclei decay toward this excited state too. ^{7}Be nuclei produced in their first excited state also give rise to a line at 0.429 MeV. Because of their Doppler broadening, these two lines melt together in a broad feature around 0.450 MeV (e.g. Murphy et al. 1990) which we refer to as the ^{7}Li-^{7}Be feature. The total emission rate is $\sim$ 40% of the total ^{7}Li production rate (e.g. RKL79).

As can be seen in Fig. 14, the ^{7}Li-^{7}Be feature (labeled as 0.450) is quite intense and probably observable for some of our EP compositions. This constitutes a distinctive prediction of our mean-wind models as compared with late-WC EP composition, for which the gamma-ray flux in the ^{7}Li-^{7}Be feature is very low, notably below INTEGRAL's thresholds. This is because the surface composition of completely evolved WC stars is much poorer in helium than the WC wind itself. In the case of models E, i.e. with enhanced mass loss rates during the MS phase, the flux in the ^{7}Li-^{7}Be feature is even higher than the flux in the 6.129 MeV line of ^{16}O. This is also true for models C at twice solar metallicity and with an EPs' injection break energy between 8 and 20 MeV/n.

In any case, we predict a flux of 1-2 10^{-5} ph.cm^{-2}s^{-1} at $\sim$ 0.450 MeV from the Orion complex, which is below the current OSSE upper limit, but above INTEGRAL's expected sensitivity.

7.2. The ^{10}B spallation lines at 0.717 MeV and 1.023 MeV

The spallation product ^{10}B can also be generated, either directly or from the decay of ^{10}C, through several excited levels, the most probable being at 0.717 MeV (RKL79). As we show in Fig. 14, the gamma-ray flux in the resulting de-excitation line should be rather intense ($\sim\ 10^{-5}$ ph.cm^{-2}.s^{-1}), especially for high values of E_0. However, the main contributions to this line are the inverse reactions ^{12}C + α and, to a lower extent, ^{16}O + α, so that the line should be broad, lowering the INTEGRAL SPI sensitivity by about a factor of 10.

Comparing the 0.717 MeV line fluxes for solar and twice solar metallicities, one can see that the (0.717 MeV)/(4.438 MeV) line ratio is unchanged. This is because both of these lines are produced by the same collisions, namely ^{12}C + $\alpha \rightarrow$ X. However, this line ratio depends on the EP spectrum, because the threshold energy is higher for the 0.717 MeV line production than for ^{12}C excitation.

The same behavior is observed at a slightly lower level for the 1.023 MeV line, resulting from the de-excitation of another level of ^{10}B (see Fig. 14).

7.3. What about the ^{11}B spallation lines?

In the light of the two preceding sections, we point out that the spallation reactions induced by the EPs should also lead to rather intense de-excitation lines from ^{11}B, since the production rate of this isotope is always greater than that of ^{10}B by a factor of 2.5 or more. It is even greater than the ^{7}Li production rate for EP spectra with $E_0 \gtrsim 30$ MeV/n.

In the case of ^{11}B, measurements have been made for the main reaction, ^{12}C$(p, 2p)^{11}$B, at a bombarding energy of 50

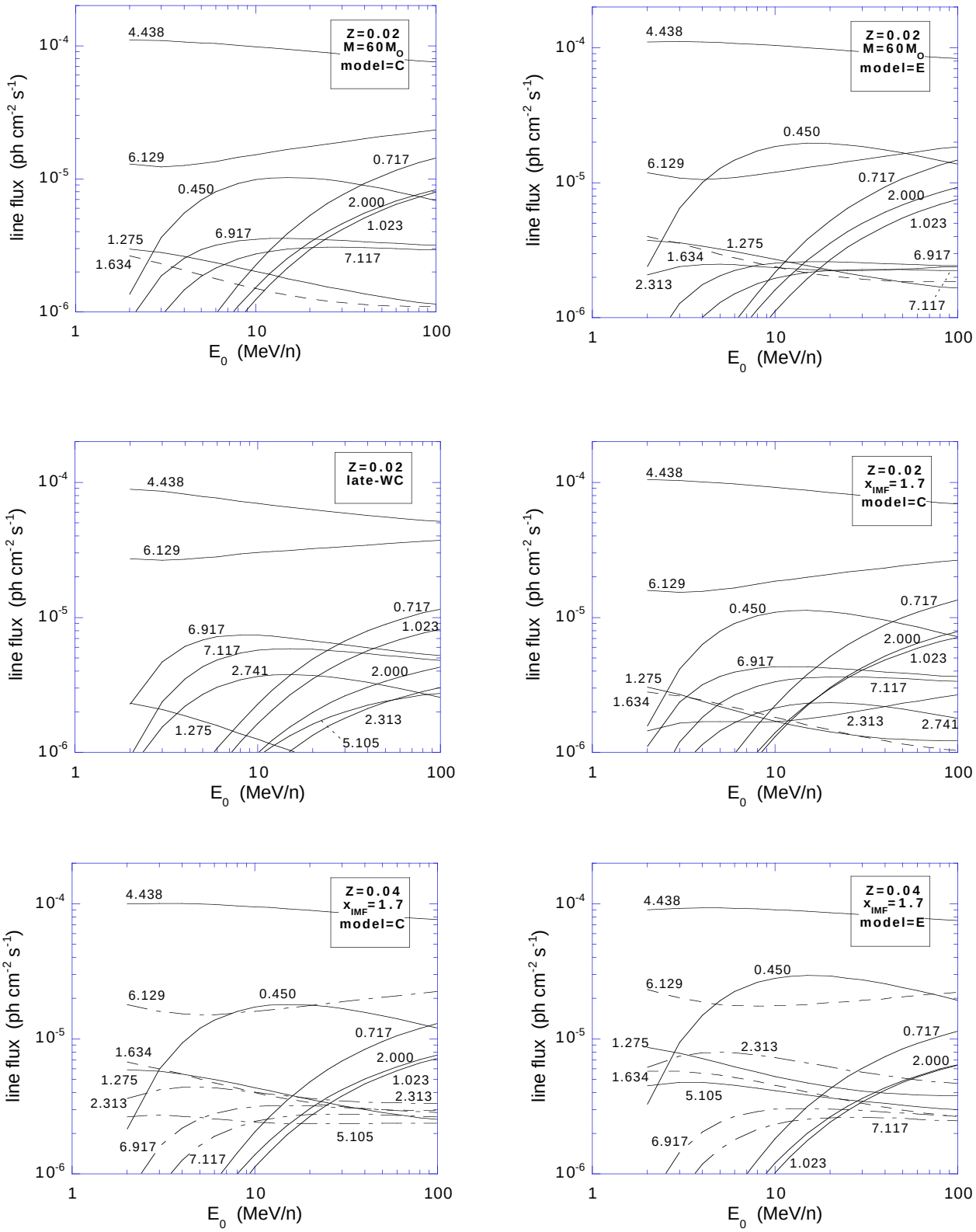

Fig. 14. Gamma-ray fluxes of the most intense lines arising from EPs-ISM interactions as a function of the injection energy break E_0, for different compositions and metallicities. The numbers labeling the curves indicate the energy (in MeV) of the gamma-ray line in the rest frame of the emitting nuclei. Solid lines correspond to the cases when the inverse process (broad line component) dominates, and dashed lines when the direct process does (narrow line component). In the case when both components are approximately equal, we use alternate dashed lines.

MeV, showing evidence for gamma-ray emission from four excited levels at 2.12, 4.45, 5.01 and 6.79 MeV, with approximately equal fluxes (Pugh et al. 1967). RKL79 also include lines from ^{11}B spallation, using some cross sections of Zobel et al. (1968), but with large uncertainties, up to a factor of 10 near the resonance peak at $\sim$ 30-40 MeV/n. We used their estimates to calculate the gamma-ray flux emitted near 2 MeV as a result of ^{12}C spallation. One component comes from ^{11}B de-excitation (2.124 MeV), and a second one comes from ^{11}C de-excitation (1.995 MeV) preceding the decay toward ^{11}B. The sum of these two components is shown in Fig. 14 with the label 2.000. The fluxes are quite low ($\lesssim 10^{-5}$ ph.cm^{-2}.s^{-1}). However, these estimates are very uncertain and new measurements of these cross sections, especially near the reaction thresholds, would be of great astrophysical interest. In Orion, if one assumes that a significant fraction of ^{11}B is actually produced in an excited state (as ^{7}Li), then the de-excitation fluxes should be of order a few 10^{-5} ph.cm^{-2}.s^{-1} and could even provide a non negligible contribution to the detected flux in the 3-7 MeV band.

7.4. Other ^{16}O lines

Fig. 14 also shows the contributions of two additional lines from the excited states at 6.917 and 7.117 MeV of ^{16}O. The emitted fluxes in these lines are of course lower than that arising from the first excited state, but would be among the most intense lines in the case when the ^{12}C*/^{16}O* line ratio is close to unity, i.e. for compositions with ^{12}C $\lesssim ^{16}$O, like solar (SS), dust grain (GR), SN35 or late-WC compositions, but unlike our mean wind compositions. For the sake of completeness, we also mention the 2.741 MeV line arising from the partial de-excitation of the 8.872 MeV level of ^{16}O toward the 6.129 level, with a branching ratio of 84% (Lederer et al. 1978). The gamma-ray flux in this line reaches $\sim 4\,10^{-6}$ ph.cm^{-2}.s^{-1} (with the 'Orion normalisation') for the late-WC composition, and $\sim 6\,10^{-6}$ ph.cm^{-2}.s^{-1} for the GR composition (not shown here).

Concerning the line width, all that we said for the 6.129 MeV line (see Sect. 6.2) holds also for the other ^{16}O lines.

7.5. The ^{14}N lines at 2.313 and 5.105 MeV

The first excited level of ^{14}N is at 2.313 MeV. It can be reached either by direct excitation or by spallation reactions involving ^{16}O nuclei. As can be seen in Fig. 14, the gamma-ray flux in the corresponding de-excitation line is always low: $\leq 3\,10^{-6}$ ph.cm^{-2}.s^{-1} with the Orion normalisation. This is due to the low ^{14}N abundance in the EPs, a consequence of the smaller contribution of the WN phase than the WC phase to the total stellar wind. One exception should however be noted, for the model with twice solar metallicity and an enhanced mass loss rate during the MS phase and, precisely, the WNL phase. In this case, the gamma-ray line flux reaches $8\,10^{-6}$ ph.cm^{-2}.s^{-1} for small values of the break energy E_0.

An additional line at 5.105 MeV has also been considered by RKL79, and we therefore included it. It corresponds to the fourth excited level of ^{14}N (Lederer et al 1978). The corresponding flux is therefore always smaller than that of the 2.313 MeV line, and should not be detectable, expect for exceptionaly ^{14}N rich compositions. Note however that ^{14}N has two other levels at 3.948 MeV and 4.915 MeV, which should provide gamma-ray fluxes larger than that in the line at 5.105 MeV, and contribute to the total emission between 3 and 7 MeV. Unfortunately, the corresponding excitation cross sections are lacking.

7.6. ^{20}Ne and ^{22}Ne lines

Neon is known to have two isotopes (^{20}Ne and ^{22}Ne) characterised by distinct production mechanisms. This makes this element very interesting in the context of nucleosynthesis. Indeed, ^{22}Ne is produced during the helium burning phase from the ^{14}N nuclei (synthesized in the CNO cycle during the H burning phase), while ^{20}Ne is produced from ^{16}O during the carbon and the oxygen burning phases. As a consequence, since the winds of W-R stars only eject elements resulting from the helium burning, no freshly synthesized ^{20}Ne nuclei are present in the mean-wind (or mean-OB) compositions.

Indeed, as can be checked from Table 1, the EP compositions that we propose are richer in ^{22}Ne than in ^{20}Ne, whereas the usual ISM composition, i.e. solar, is made of about 10 times more ^{20}Ne than ^{22}Ne. The detection of the ^{22}Ne line at 1.275 MeV at the same flux as the ^{20}Ne line at 1.634 MeV would therefore constitute a clear signature of the link between the winds of Wolf-Rayet stars and the EPs.

Unfortunately, both lines have rather low fluxes, and should not be detected as individual lines. We further note that even in the hypothetical case of a ^{20}Ne line detection, the absence of the ^{22}Ne line would not be conclusive. Indeed, while both lines are expected to have approximately equal fluxes for all our mean wind compositions, the ^{20}Ne line is always narrow (due to the excitation of ^{20}Ne nuclei in the ISM) contrary to the ^{22}Ne line, which is broad (due to the ^{22}Ne nuclei in the EPs) and most certainly swamped in the rest of the gamma-ray emission.

8. Influence of the assumed limit mass $M_{\rm inf}$

As discussed in Sect. 2.2, the EPs accelerated within a superbubble energized by strong stellar winds and SN explosions should be made of the wind ejecta of the most massive stars ($M \geq 40\,{\rm M}_\odot$) in the OB association responsible for the creation of the superbubble. However, this limit mass is admitedly somewhat arbitrary. To be general, we thus did the same calculations as above with EP compositions which include all the stars with a mass greater than $M_{\rm inf} = 20\,{\rm M}_\odot$. This is considered as an extreme case.

As expected from the resulting lower abundances of C and O (see Sect. 2.2), we obtain a (1-3 MeV)/(3-7 MeV) band ratio, R, some 20 to 30 % higher than with $M_{\rm inf} = 40\,{\rm M}_\odot$ for models C, while R is virtually unchanged for models E. In particular, all the mean-wind and mean-OB compositions still satisfy the Orion constraint $R \leq 0.13$, whatever the value of $M_{\rm inf}$. The same quantitative changes (+ 20-30% for models C; no change

for models E) are also obtained for the (0.2-1 MeV)/(3-7 MeV) band ratio.

Concerning the $^{12}C^*/^{16}O^*$ line ratio, we find a value $\sim 10\%$ lower for model C at solar metallicity, and $\sim 50\%$ lower for model C at twice solar metallicity. This is a consequence of the lower C/O abundance ratio in the EP composition. Finally, we obtain smaller broad-to-narrow line component ratios (i.e. narrower lines), as expected again from the lower abundance of C and O in the EPs, favouring the direct processes. Quantitatively, we find values $\sim 50\%$ smaller for the ^{12}C line and $\sim 30\%$ smaller for the ^{16}O line, at either solar and twice solar metallicity.

9. Summary

We have calculated the gamma-ray line production induced by energetic particles (EPs) in active molecular clouds, assuming that the composition of the EPs reflects that of the combined wind material of Wolf-Rayet stars (W-R). The resulting composition is found to be enriched in C and O, but not completely devoid of protons and α particles, which ensures a non negligible contribution of the narrow line component to the induced nuclear de-excitation lines.

As far as Orion is concerned, we have shown that any of our mean-wind or mean-OB compositions satisfies the observational constraint provided by the COMPTEL measurement of the (1-3 MeV)/(3-7 MeV) band ratio, R. Our calculations also revealed the importance of the unresolved gamma-ray lines from nuclei heavier than ^{20}Ne, since the exclusion of specific EP compositions (such as SS or CRS) on the basis of the R band ratio actually depends on the distribution of these unresolved lines in the energy range (0.7-7 MeV). Accurate measurements of the corresponding cross sections would therefore be of astrophysical interest. We found that the $^{12}C^*/^{16}O^*$ line ratio obtained with SS, GR, SN35 and late-WC compositions is hardly compatible with estimates from COMPTEL's data. By contrast, our mean-wind and mean-OB compositions seem to satisfy all the available constraints. Similarly, we found that the inverse-to-direct component ratio is very sensitive to the assumed EP composition, and therefore represents a powerful observational constraint.

We have shown that the ^{16}O line should be significantly narrower than the ^{12}C line, because of the larger contribution of the inverse reactions. The ^{16}O narrow line component should even dominate at twice solar metallicity, which is relevant to the gamma-ray emission from the inner Galaxy. Moreover, both (0.2-1 MeV)/(3-7 MeV) and (1-3 MeV)/(3-7 MeV) band ratios are larger by a factor of 1.5-3 at twice solar metallicity, so that we predict a variation with Galactic longitude of the gamma-ray line spectrum, of interest for the INTEGRAL mission.

We also found that the gamma-ray emission in the ^{7}Li-^{7}Be feature at ~ 0.450 MeV should be measurable by INTEGRAL in Orion, with a flux of $\sim 10^{-5}$ ph.cm^{-2}s^{-1}. This flux, as compared to that in the (3-7 MeV) band, should intensify toward the inner regions of the Galaxy by a factor of about 2. Other spallation lines should provide a significant contribution to the gamma-ray emission at MeV energies, like the ^{10}B line at 0.717 MeV which even exceeds the ^{16}O line for high values of the injection break energy E_0. In this respect, measurements of the production cross sections of excited fragments would be of great astrophysical interest. Indeed, in light of our calculations, the future detection of a ^{11}B line of spallative origin is not unrealistic. This would provide a 'live record' of ongoing spallative nucleosynthesis of light elements in the ISM.

Acknowledgements. We wish to thank R. Lehoucq warmly for his first version of the code that we used to calculate the nuclear reaction rates. We also thank Reuven Ramaty for details on the unresolved gamma-ray lines. We are grateful to Jurgen Kiener for providing us with accurate tables of energy loss rates. This work has been done in the framework of the PICS 'Nuclear gamma-ray lines and associated nucleosynthesis'.

References

Blaauw, A., 1964, ARA&A 2, 213
Bloemen, H., et al., 1984, A&A 139, 37
Bloemen, H., et al., 1994, A&A 281, L5
Bloemen, H., et al., 1997, ApJ 475, L25
Brown, A.G.A., de Geus, E.J. and de Zeeuw, P.T., 1994, A&A 289, 101
Burrows, D.N., Singh, K.P., Nousek, J.A., Garmire, G.P. and Good, J., 1993, ApJ 406, 97
Bykov, A.M., 1995, Space Sci. Rev. 74, 397
Bykov, A.M. and Bloemen, H., 1994, A&A 281, L1
Bykov, A.M. and Fleishman, G.D., 1992, MNRAS 255, 269
Bykov, A.M. and Toptygin, I.N., 1990, Sov. Phys. JETP 71, 702
Bykov, A.M., Bozhokin, S.V. and Bloemen, H., 1996, A&A 307, L37
Cassé, M., Lehoucq, R. and Vangioni-Flam, E., 1995, Nature 373, 318
Cowie, L.L., Songaila, A. and York, D.G., 1979, ApJ 230, 469
Digel, S.W., Hunter, S.D. and Mukherjee, R., 1995, ApJ 441, 270
Ellison, D.C., Drury, L.O'C. and Meyer, J.-P., 1997, ApJ, in press
Ellison, D.C., and Ramaty, R., 1985, ApJ 298, 400
Lamers, H.J.G.L.M. and Leitherer, C., 1993, ApJ 412, 771
Lederer, C.M., Shirley, V.S. and Browne, E., 1978, Table of isotopes, 7th ed. Wiley (New York)
Meyer, J.-P., Drury, L.O'C. and Ellison, D.C., 1997, ApJ, in press
Meynet, G., Maeder, A., Schaller, G., Schaerer, D. and Charbonnel, C., 1994, A&AS, 103, 97
Murphy, R.J., Hua, X.-M., Kozlovsky, B. and Ramaty, R., 1990, ApJ 351, 299
Murphy, R.J., Ramaty, R., Kozlovsky, B. and Reames, D.V., 1991, ApJ 371, 793
Parizot, E.M.G., 1997, A&A submitted
Parizot, E.M.G., Lehoucq, R., Cassé, M. and Ellison, D.C., 1997, in 'The Transparent Universe' ed. C. Winkler, T.J.-L. Courvoisier and Ph. Durouchoux, ESA Publications Division, p. 93
Parizot, E.M.G., Lehoucq, R., Cassé, M. and Vangioni-Flam, E., 1997, in 'The Transparent Universe' ed. C. Winkler, T.J.-L. Courvoisier and Ph. Durouchoux, ESA Publications Division, p. 97
Parizot, E.M.G., Ellison, D.C., Lehoucq, R. and Cassé, M., 1997, in 'The Transparent Universe' ed. C. Winkler, T.J.-L. Courvoisier and Ph. Durouchoux, ESA Publications Division, p. 43
Pugh, H.G., Hendrie, D.L., Chabre, M. and Boschitz, E., 1967, Phys. Rev. 155, 4, 155
Ramaty, R., 1996, A&AS 120, 373
Ramaty, R., Kozlovsky, B. and Lingenfelter, R.E., 1979, ApJS 40, 487 (RKL79)

Ramaty, R., Kozlovsky, B. and Lingenfelter, R.E., 1995, ApJ 438, L21
Ramaty, R., Kozlovsky, B. and Lingenfelter, R.E., 1996, ApJ 456, 525 (RKL96)
Ramaty, R., Mandzhavidze, N., Barat, C. and Trottet, G., 1997, ApJ 479, 458
Ramaty, R., Kozlovsky, B. and Lingenfelter, R.E., 1997, in 'The Transparent Universe' ed. C. Winkler, T.J.-L. Courvoisier and Ph. Durouchoux, ESA Publications Division, p. 75
Schaller, G., Schaerer, D., Meynet, G. and Maeder, A., 1992, A&AS 96, 269
Tatischeff, V., Cassé, M., Kiener, J., Thibaud, J.-P. and Vangioni-Flam, E., 1996, ApJ 472, 205
Vangioni-Flam, E., Cassé, M., Fields, B. and Olive, K.A., 1996, ApJ 468, 199
Vangioni-Flam, E., Cassé, M. and Ramaty, R., 1997, in 'The Transparent Universe' ed. C. Winkler, T.J.-L. Courvoisier and Ph. Durouchoux, ESA Publications Division, p. 123
Vilkoviskij, E.Ya. and Tambovtseva, L.V., 1992, A&AS 94, 109
Woosley, S.E., Langer, N. and Weaver, T.A., 1993, ApJ 411, 823
Zobel, W., Maienschein, F.C., Todd, J.H. and Chapman, G.T. 1968, Nucl. Sci. Eng. 32,392

This article was processed by the author using Springer-Verlag LaTeX A&A style file *L-AA* version 3.